Localization-Dependent Photoluminescence Spectrum of Biexcitons in Semiconductor Quantum Wires

A. Feltrin,* F. Michelini,† J. L. Staehli, and B. Deveaud
Institut de Photonique et d'Électronique Quantiques, École Polytechnique Fédérale de Lausanne (EPFL), CH-1015 Lausanne, Switzerland

V. Savona
Institut de Théorie des Phénomènes Physiques, École Polytechnique Fédérale de Lausanne (EPFL), CH-1015 Lausanne, Switzerland

J. Toquant
Institute of Physics, University of Basel, Klingelbergstrasse 82, CH-4056 Basel, Switzerland

X. L. Wang and M. Ogura
Photonics Research Institute, National Institute of Advanced Industrial Science and Technology, Tsukuba Central 2, Tsukuba 305-8568, Japan

(Received 15 June 2005; published 20 October 2005)

We study exciton and biexciton spectra in disordered semiconductor quantum wires by means of nanophotoluminescence spectroscopy. We demonstrate a close link between the exciton localization length along the wire and the occurrence of a biexciton spectral line. The biexciton signature appears only if the corresponding exciton state extends over more than a few tens of nanometers. We also measure a nonmonotonous variation of the biexciton binding energy with decreasing exciton localization length. This behavior is quantitatively well reproduced by the solution of the single-band Schrödinger equation of the four-particle problem in a one-dimensional confining potential.

DOI: 10.1103/PhysRevLett.95.177404 PACS numbers: 78.67.Lt, 68.37.Uv, 73.21.Hb, 78.55.Cr

Photoexcited electron-hole pairs in semiconductors can form hydrogenlike bound states called excitons. If the photoexcitation is strong enough, the formation of molecules made of two excitons, called biexcitons, becomes possible [1]. Recently, exciton-biexciton systems have attracted considerable interest because they represent a model system for the implementation of elementary quantum computing operations [2] and because of their potential as sources of strongly correlated photon pairs both in bulk materials [3] and in quantum confined nanostructures [4]. Works on biexciton properties in nanostructures have studied its internal structure, binding energy, and dependence on dimensionality [5] and structural disorder [6–8].

In presence of heterointerface disorder, a biexciton signature in the emission spectrum appears only in the case of exceptionally large Coulomb correlation energy [9]. In most cases of *III-V* heterostructures, however, disorder can broaden the excitonic resonance by an amount comparable or larger than the biexcitonic binding energy, thus hiding the biexcitonic spectral feature. Consequently, either nonlinear spectroscopic techniques, as four-wave mixing, or μm (or nano)photoluminescence (PL) become necessary in order to detect a biexciton signature [2,10–12]. In most nano-PL studies (see, e.g., Ref. [13]), however, the biexciton spectral feature tends to be absent. It has been speculated that exciton localization might play a role in explaining this lack of biexcitonic emission [14], but until now no systematic study has been undertaken.

In this context, another long standing issue has been the disagreement, especially in quantum wells, between theoretical predictions and experimental measurements of the biexciton binding energy [15,16]. Remarkably, most of the theoretical studies have concentrated on the quantum well case [6–8], whereas none, to the best of our knowledge, has been devoted to quantum wires (QWRs).

In this Letter, we study biexciton states in QWRs as a function of exciton localization. To this purpose, we employ a nanophotoluminescence experimental technique able of high spatial resolution. We present the first experimental evidence in a disordered QWR system that the presence or absence of the biexciton emission in nano-PL spectra is related to the exciton localization length. In addition, we study the dependence of the biexciton binding energy upon the exciton localization, finding that more localized states present a larger energy spread of the biexciton binding energy, than more extended ones. Our measurements are supported by a model relying on the solution of the four-particle, one-dimensional biexciton Schrödinger equation in the effective-mass approximation. This model explains the dependence of the biexciton binding energy on localization and agrees well with the experimental data.

The experimental apparatus is a low temperature (8 K) scanning near-field optical microscope (SNOM) [17]. The excitation source is the 530.9 nm line of a Kr^+ laser, and the PL signal is analyzed by a double monochromator

(25 μeV spectral resolution), a photomultiplier tube for spectrally integrated acquisitions over the scanning area, and a cooled CCD camera for spectral acquisitions at a given position. All measurements are performed in the excitation-collection mode with a chemically etched uncoated single mode fiber with an overall spatial resolution of 200 nm.

The investigated samples are $GaAs/Al_{0.33}Ga_{0.67}As$ V-groove QWRs [18,19]. The far-field PL spectrum exhibits a full width at half maximum of 8 meV, due to inhomogeneous broadening. Near-field PL spectra show some domains of very high interface quality, where exciton states extend over hundreds of nanometers along the wire. As in previous analyses [10], we will distinguish spatial domains of type A, displaying only one exciton line, from those of type B where more than one sharp exciton peak appears within the SNOM resolution in the low-excitation nano-PL spectrum.

For type A spatial domains, our analysis proceeds as follows. First, we measure the spatial extension of single exciton PL peaks at low-excitation intensity, where inter-excitonic interactions are negligible. In our interpretation, we identify the extension over which the PL intensity remains approximatively constant with the extension of the exciton center-of-mass (c.m.) wave function. As an example we show in Fig. 1(a) near-field spectra as a function of the tip position along the QWR for the most extended exciton state we measured. Second, we place the fiber tip at the center of the domain, increase the excitation intensity, and a new line appears on the low energy side of the exciton peak [Fig. 1(b)]. We attribute this emission line to the biexciton state. This attribution is based on the analysis of the integrated emission intensity of the two lines as a function of the excitation intensity, as can be seen in Fig. 1(c): to an almost linear increase of the exciton PL intensity corresponds a quadratic increase of the biexciton intensity. The binding energy of the biexciton is given by the energy separation between the exciton and the biexciton peak. In this case it is $B_{BX} = 2.075$ meV. We stress the fact that in *all* QWR domains whose size is large enough to display a single exciton peak, we *always* observe a single biexciton line upon increasing the excitation, providing further evidence of its biexcitonic origin [10]. The alternative explanation in terms of neutral or charged exciton states bound to impurities can be ruled out not only on the basis of the different expected power dependence, but also because they could generally give rise to more than one additional spectral line (or even to none) for each exciton line, according to the local impurity environment.

In the case of type B domains, a rough estimate of the exciton localization lengths is given by the ratio between the SNOM spatial resolution and the number of measured peaks. This sets the values to a few tens of nanometers. To illustrate the trend, we focus here on three nano-PL spectra, respectively, having five, seven, and nine PL peaks at low-

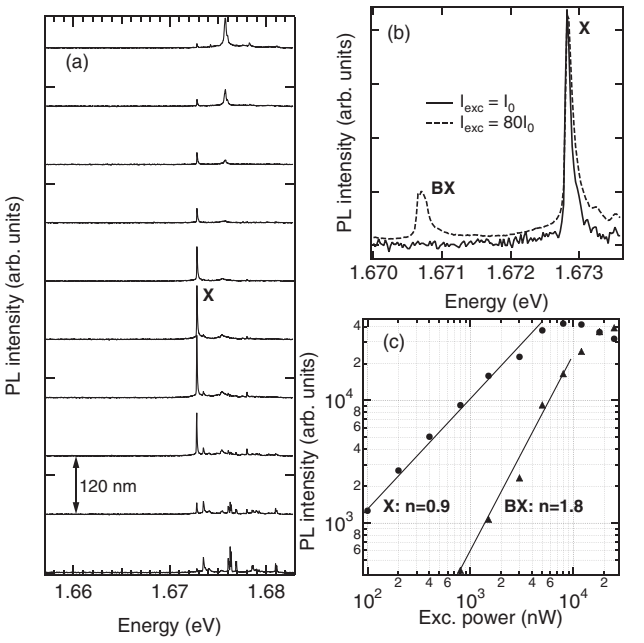

FIG. 1. (a) Near-field spectra taken at low-excitation intensity ($I_0 = 10$ mW cm^{-2}) and at regular spatial intervals of 120 nm along the QWR in a spatial domain of type A, indicating an extension of about 300 nm for the exciton line. (b) Two near-field spectra taken at the center of this domain for different excitation intensities, showing the presence of an additional line at high excitation. (c) Log-log plot of the integrated intensity dependence on the laser power of the exciton and biexciton emission lines. Fits to a power law $I_{PL} \propto I_{exc}^{n}$ are also plotted.

excitation intensity. All other measured spectra show the same general behavior. For the case of five exciton peaks [Fig. 2(a)], five supplementary peaks appear as the excitation is increased. The systematic appearance of these additional lines and their quadratic dependence on the excitation intensity again allows one to relate them to biexcitons. For one of the exciton peaks [Fig. 2(d)], a supplementary line appears on the high energy side of one of the exciton lines, suggesting a negative binding energy of $B_{BX} = -0.975$ meV. Apart from this isolated case, the other binding energies range between 2.025 and 2.65 meV. For the case with seven emission lines [Fig. 2(b)], only one additional line appears for increasing excitation. Finally in the case of nine lines [Fig. 2(c)], no additional peaks appear. The data therefore suggest that for QWR domains of type B displaying an increasing number of exciton peaks—and therefore a decreasing average exciton localization length—the biexciton emission peaks tend to disappear.

The results concerning the binding energy are summarized in Fig. 3. Because of the limited spatial resolution of the SNOM, we can only distinguish between states having an extension comparable or larger than 200 nm. We attribute to all other experimental points a nominal localization length of 50 nm, which refer to measurements done in

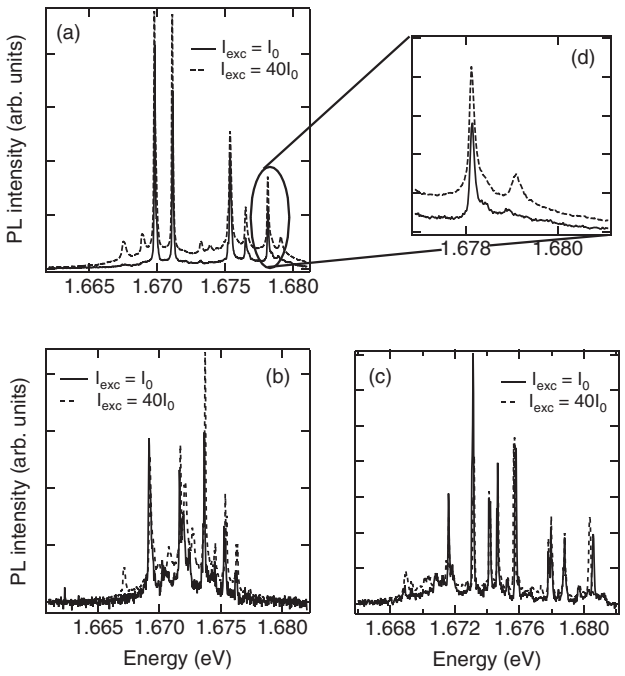

FIG. 2. Near-field spectra taken in three different QWR domains of type B and for two different excitation intensities ($I_0 = 10\ \mathrm{mW\,cm^{-2}}$), where, respectively, (a) five, (b) seven, and (c) nine exciton lines are present at low-excitation intensity, but (a) five, (b) one, or (c) no additional line appear upon increasing the excitation intensity. Spectrum (d) shows more clearly the additional peak emerging on the *high energy side* of one exciton peak in spectrum (a).

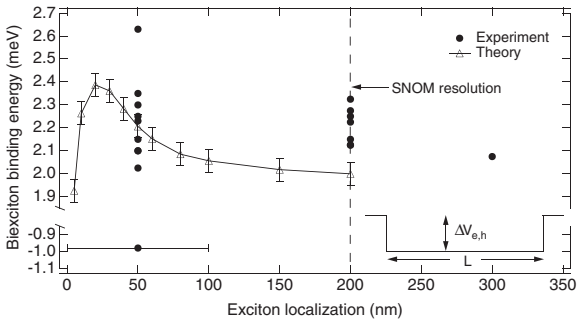

FIG. 3. Measured biexciton binding energies as a function of the estimated exciton localization lengths (solid dots). The horizontal error bar applies to all experimental points and are determined by the spatial step of 120 nm between two successive spectra. We also plot the calculated biexciton binding energies (triangles) for a one monolayer deep single particle square localization potential (see inset). The vertical error bars are due to the tolerance of the numerical results. The parameters used were $\delta V_e = 4.9$ meV, $\delta V_h = 1.1$ meV, $m_e = 0.067m_0$, and $m_h = 0.26m_0$. m_0 is the free electron mass.

QWR domains of type B. It appears very clearly that extended states are less affected by changes in the localization length, whereas more localized states show larger variations of the biexciton binding energy.

For the theoretical model, we start from the three-dimensional effective-mass Schrödinger equation for two electrons and two holes. As the intersubband energy separation is much larger than both the amplitude of disorder energy fluctuations, the exciton, and the biexciton binding energy [20], we can safely employ the single-subband approximation. This consists in neglecting the mixing of higher electron and hole subbands in the exciton and biexciton states. The biexciton wave function Ψ_α, in particular, is rewritten as follows: $\Psi_\alpha(\mathbf{r}_{e1}, \mathbf{r}_{e2}, \mathbf{r}_{h1}, \mathbf{r}_{h2}) = \Phi(z_{e1}, z_{e2}, z_{h1}, z_{h2}) \prod_a u_a(\mathbf{r}_a^\perp)$, with a running over the four-particle indexes $e1$, $e2$, $h1$, $h2$. The functions u_a are the single-particle confinement wave functions of ground electron and hole subband states in the direction transverse to the QWR. Integrating the three-dimensional Schrödinger equation over the transverse coordinates $\mathbf{r}_a^\perp$, reduces it to an effective one-dimensional equation:

$$\left[\sum_a \left(\frac{-\hbar^2}{2m_a}\frac{d^2}{dz_a^2} + V_a(z_a) + \sum_{b\neq a} U_a^b(z_a - z_b)\right) - E_{\mathrm{BX}}\right]\Phi = 0.$$

E_{BX} is the biexciton energy. $V_a(z_a)$ represents the single-particle confinement potential due to a monolayer step heterointerface fluctuation along the QWR axis [20].

The equation contains six Coulomb terms, four attractive and two repulsive. Strictly speaking, the spatial dependence of $U_a^b(z)$ on z depends on the particles a and b. However, inspection of QWR electron and hole confinement functions show that these differences are small [21] and we will neglect them, approximating all Coulomb terms by the following expression:

$$U_a^b(z) = \frac{e^2\sigma_a^b}{4\pi\epsilon\epsilon_0}\frac{1}{|z| + l_0}. \quad (1)$$

σ_a^b takes the values $\pm 1/2$, depending on the charges of the particles. A detailed discussion about the approximation of Eq. (1) can be found in Ref. [22]. l_0 is a free parameter related to the exciton binding energy which is difficult to measure experimentally in our sample. We thus take the theoretical result of Ref. [23], $E_{\mathrm{X}} = -17$ meV, and adjust l_0 to reproduce it, obtaining $l_0 = 3$ nm.

We choose a square shape of the single-particle potential $V_a(z_a)$ (see inset of Fig. 3), neglecting the contribution of alloy disorder. In order to calculate the biexciton binding energy it is necessary to solve first the corresponding exciton problem. The binding energy is then calculated as $B_{\mathrm{BX}} = 2E_{\mathrm{X}} - E_{\mathrm{BX}}$. Both exciton (two-particle) and biexciton (four-particle) one-dimensional Schrödinger equations were solved numerically on a discrete grid in real space, using a parallel computation facility. The simulation was performed on a QWR length of 200 nm with infinite well boundary conditions, and the convergence of both exciton and biexciton eigenenergies versus grid step-size was carefully checked.

The computed biexciton binding energy is plotted in Fig. 3 as a function of the dip size for a one monolayer deep width fluctuation (see inset). Very good agreement with the corresponding measured values is obtained. We observe an increase of the biexciton binding energy as the size of the dip shortens, followed by a decrease for the smallest dip sizes. We remark that, in the calculations, the binding energy increases by about 0.4 meV, which is slightly smaller than the variation seen in the experiment. Qualitatively similar results were obtained in the case of a two monolayer deep well.

Our results are qualitatively very similar to the ones obtained in Ref. [8]. We discuss the computed biexciton binding energy for decreasing dip size, starting from the largest computed value $L = 200$ nm. For sufficiently large dip sizes, as compared to the mean distances between the bound electrons and holes, we expect both exciton and biexciton to behave as rigid particles. We then assume, as is usually done for the exciton in disordered nanostructures, that the localization potential acts only on the c.m. part of the wave function, without affecting the internal motion. This is the limit treated in Ref. [7]. It is then possible to rewrite B_{BX} in the following way: $B_{\mathrm{BX}} = (2K_{\mathrm{X}} - K_{\mathrm{BX}}) + B_{\mathrm{BX}}^{\infty}$. K_{X} (K_{BX}) is the exciton (biexciton) c.m. kinetic term, and B_{BX}^{∞} is the binding energy of the biexciton in an ideal QWR and is a constant term. Thus at first the variation in the biexciton binding energy B_{BX} is due to the kinetic terms. This leads to an increase of the biexciton binding energy because the exciton term counts twice and because the exciton has a mass which is half the biexciton mass: the exciton kinetic contribution is more sensitive to variations of the dip size. The decrease for the smallest dip sizes is on the contrary due to changes in the internal motion in the biexciton, in particular, to the hole-hole Coulomb repulsion. Because of the hole heavier mass, as compared to electrons, the hole charge density is more peaked and leads to a strong repulsion when the biexciton is forced into very small dips. Indeed, calculations done for the same dip sizes but with smaller hole masses (i.e., wider charge distributions) show no decrease of B_{BX}.

Our model describes in a satisfactory way the experimental biexciton binding energies, except for the single observed negative one. Until now negative binding energies have been observed only in strongly confined quantum dots [24], where they are attributed to the strong spatial confinement causing the direct Coulomb repulsion to outbalance the attractive contributions to the binding energy. In our case, however, the spatial confinement is weaker and the binding contribution is expected to dominate. We do not understand at present the physical origin of this isolated experimental evidence. It might be argued that carrier density effects [25] can make the biexciton system behave in a substantially different way from the simple four-particle picture adopted in our mode. Alternatively, the presence of locally excited states and the interplay between biexciton formation dynamics and localization might also be considered.

In conclusion, we studied the relationship between exciton localization and biexciton binding energy in quantum wires and we showed that the presence of the biexciton peak in near-field spectra depends critically on the exciton localization length. These results shine new light on the biexciton localization properties which go beyond the specific case of QWRs. By solving the four-particle Schrödinger equation, we were able to compute the binding energy of the localized biexciton. It displays a nonmonotonous dependence on the dip size, in good agreement with our measurements.

We are grateful to M.-A. Dupertuis for enlightening discussions. A. F. and V. S. acknowledge financial support from the Swiss National Science Foundation, through Projects No. 2000-067061 and No. 620-066060.

*Present address: Photovoltaics and Nanostructures Group, TCAM, University of Houston, Houston, TX 77204-5004, USA.

†Present address: Laboratory for Material and Microelectronics of Provence, UMR CNRS 6137, 13384 Marseille Cedex 13, France.

[1] W. F. Brinkman *et al.*, Phys. Rev. B **8**, 1570 (1973).
[2] W. Q. Li *et al.*, Science **301**, 809 (2003).
[3] K. Edamatsu *et al.*, Nature (London) **431**, 167 (2004).
[4] E. Moreau *et al.*, Phys. Rev. Lett. **87**, 183601 (2001).
[5] J. Usukura, Y. Suzuki, and K. Varga, Phys. Rev. B **59**, 5652 (1999).
[6] O. Heller, P. Lelong, and G. Bastard, Phys. Rev. B **56**, 4702 (1997).
[7] O. Mayrock *et al.*, Phys. Rev. B **60**, 5582 (1999).
[8] A. V. Filinov *et al.*, Phys. Rev. B **70**, 035323 (2004).
[9] F. Kreller *et al.*, Phys. Rev. Lett. **75**, 2420 (1995).
[10] K. Brunner *et al.*, Phys. Rev. Lett. **73**, 1138 (1994).
[11] A. Crottini *et al.*, Solid State Commun. **121**, 401 (2002).
[12] T. Guillet *et al.*, Phys. Rev. B **67**, 235324 (2003).
[13] F. Intonti *et al.*, Phys. Rev. Lett. **87**, 076801 (2001).
[14] C. Piermarocchi and C. Lienau (private communication).
[15] W. Langbein and J. M. Hvam, Phys. Rev. B **59**, 15 405 (1999).
[16] W. Langbein *et al.*, Phys. Status Solidi A **190**, 167 (2002).
[17] A. Crottini *et al.*, Ultramicroscopy **90**, 97 (2002).
[18] X. L. Wang *et al.*, Appl. Phys. Lett. **66**, 1506 (1995).
[19] G. Biasiol and E. Kapon, Phys. Rev. Lett. **81**, 2962 (1998).
[20] R. Zimmermann *et al.*, in *Quantum Coherence, Correlation and Decoherence in Semiconductor Nanostructures* (Academic Press, London, 2003), pp. 89–165.
[21] M.-A. Dupertuis (private communication).
[22] M. Combescot *et al.*, Eur. Phys. J. B **34**, 9 (2003).
[23] A. Siarkos and E. Runge, Phys. Rev. B **61**, 16 854 (2000).
[24] S. Rodt *et al.*, Phys. Rev. B **68**, 035331 (2003).
[25] F. Tassone and C. Piermarocchi, Phys. Rev. Lett. **82**, 843 (1999).